

# Search for Neutrino Transients Using IceCube and DeepCore

A Thesis  
Presented to  
The Academic Faculty

by

**Jacob D. Daughhetee**

In Partial Fulfillment  
of the Requirements for the Degree  
Doctor of Philosophy

School of Physics  
Georgia Institute of Technology  
January 2014

# **Search for Neutrino Transients Using IceCube and DeepCore**

Approved by:

Professor Pablo Laguna, Committee  
Chair

Professor Sven Simon  
(Earth and Atmospheric Science)

Professor Ignacio Taboada, Adviser

Professor John Wise

Professor Nepomuk Otte

Date Approved \_\_\_\_\_



## PREFACE

This dissertation is based on data acquired with the IceCube Neutrino Observatory whose maintenance and operation is the result of an immense international collaborative effort. The bulk of the work pertaining to experimental hardware, data acquisition, reconstruction algorithms, and simulation presented in this document can be attributed to many IceCube collaborators. However, the refinement of the event selection and subsequent analysis of the data are the original work of the author.

## **ACKNOWLEDGEMENTS**

I want to thank my fellow graduate student office mates whose constant distractions helped me retain my sanity.

## TABLE OF CONTENTS

<b>DEDICATION</b> . . . . .	iii
<b>PREFACE</b> . . . . .	iv
<b>ACKNOWLEDGEMENTS</b> . . . . .	v
<b>LIST OF TABLES</b> . . . . .	viii
<b>LIST OF FIGURES</b> . . . . .	ix
<b>SUMMARY</b> . . . . .	xi
<b>I INTRODUCTION</b> . . . . .	1
<b>II NEUTRINO PROPERTIES</b> . . . . .	2
2.1 Interactions in Matter . . . . .	2
2.1.1 Neutrino-Nucleon Scattering . . . . .	3
2.1.2 Deep Inelastic Scattering . . . . .	3
2.1.3 Propagation of Interaction Products . . . . .	3
2.2 Flavor Oscillations . . . . .	4
<b>III NEUTRINO ASTRONOMY</b> . . . . .	5
3.1 Motivation . . . . .	5
3.2 Detection Methods . . . . .	6
<b>IV NEUTRINO SOURCES</b> . . . . .	7
4.1 Active Galactic Nuclei . . . . .	7
4.2 Gamma-ray Bursts . . . . .	7
4.3 Core-Collapse Supernovae . . . . .	7
4.4 Choked Gamma-ray Bursts . . . . .	8
<b>V DETECTOR</b> . . . . .	9
5.1 IceCube and IceTop . . . . .	9
5.2 DeepCore . . . . .	11
5.3 Neutrino Events in IceCube . . . . .	12

<b>VI DATA ACQUISITION</b>	<b>17</b>
6.1 The Digital Optical Module	17
6.2 Hit Generation	18
6.3 Data Synchronization	18
6.4 Triggering and Event Building	18
<b>VII EVENT SELECTION</b>	<b>19</b>
7.1 Low-energy Channel	19
7.2 Analysis Specific Cuts	20
7.2.1 Veto Cuts	20
7.2.2 Quality Cuts	20
7.2.3 Boosted Decision Tree	20
7.3 Event Reconstruction	20
7.4 Final Level Data	20
<b>VIII ANALYSIS METHOD</b>	<b>22</b>
8.1 Unbinned Likelihood Method	22
8.2 Sky Scan	22
8.3 Significance and Trials Factors	23
<b>IX SYSTEMATIC EFFECTS</b>	<b>24</b>
9.1 Ice Properties	24
9.2 DOM Quantum Efficiency	24
<b>X RESULTS</b>	<b>25</b>
<b>XI INTERPRETATION</b>	<b>27</b>
<b>XII CONCLUSION</b>	<b>28</b>
<b>APPENDIX A — APPENDIX A – FINAL LEVEL EVENT DISTRIBUTIONS</b>	<b>29</b>
<b>INDEX</b>	<b>34</b>
<b>VITA</b>	<b>35</b>

## **LIST OF TABLES**

1	Final level data rate.	20
---	------------------------	----

## LIST OF FIGURES

2	Feynman diagram of a $\nu_\mu$ undergoing deep inelastic scattering with a nucleon via charged-current interaction. A large momentum exchange through a charged $W$ boson leads to breakup of the nucleon. . . . .	3
1	cross-sections . . . . .	3
3	Energy Fluence of $\nu_\mu$ and $\bar{\nu}_\nu$ from high-luminosity GRB at a redshift of z=0.1 [17] . . . . .	7
4	Observed SNe within 10 Mpc in the years 1999-2008 [16] . . . . .	8
5	Diagram of the IceCube Neutrino Observatory (Courtesy of the IceCube Collaboration). . . . .	10
6	Top down and side-view diagram of DeepCore. The side-view shows the difference in DOM distribution for the infill strings and their relation to the dust layer [5]. . . . .	14
7	A high-energy cascade event in IceCube with deposited energy of $210 \pm^{29.0}_{25.8}$ TeV [13]. The colored spheres represent DOMs that have registered light during the event. The size of the spheres are indicative of the total light received by the PMT on that DOM. The color denotes the timing of the hit with red corresponding to earlier times and blue corresponding to later times.	15
8	A high-energy track event in IceCube with deposited energy of $71.4 \pm 9.0$ TeV [13]. The colored spheres represent DOMs that have registered light during the event. The size of the spheres are indicative of the total light received by the PMT on that DOM. The color denotes the timing of the hit with red corresponding to earlier times and blue corresponding to later times.	16
9	Schematic detailing DOM structure [8]. . . . .	17
10	A fully assembled DOM supported by a cable harness. . . . .	17
11	Median event resolution as a function of energy for simulation events passing all cuts. . . . .	20
12	Median event resolution as a function of number of hit DOMs for simulation events passing all cuts. . . . .	20
13	Event display for a final level neutrino track event originating in DeepCore. The colored spheres represent DOMs that have registered a hit during the event. The size of the spheres are indicative of the total light received by the PMT on that DOM. The color denotes the timing of the hit with red corresponding to earlier times and blue corresponding to later times. . . . .	21
14	Randomized sky map of pre-trials p-values for best flares per bin. Random map generated by scrambling arrival times of real events. The black circle shows the location of the most significant flare found by the method. . . . .	23

15	Sky map of pre-trials p-values for best flares per bin. The black circle identifies the location of the most significant flare found at RA = 268.75° and Declination = 54.25°. . . . .	25
16	Distribution of test statistic $\lambda$ of most significant flare found in 1,985 background trials. The test statistic value for the best fit flare on the unscrambled data set is also plotted. . . . .	26

## SUMMARY

# **CHAPTER I**

## **INTRODUCTION**

The primary focus of the analysis presented in this thesis is to apply previously developed time-dependent point source search techniques to a set of neutrino events much lower in energy than has been attempted before.

# CHAPTER II

## NEUTRINO PROPERTIES

The neutrino is an electrically neutral particle that interacts only via the weak nuclear force and gravity. Its cross-section for interaction with ordinary matter is exceedingly small making the experimental detection of the neutrino a difficult task. It is classified as a lepton in the Standard Model, meaning that it is an elementary particle with  $\frac{1}{2}$ -integer spin (a fermion) and no strong force interaction. Neutrinos come in three variations with one corresponding to each of the three charged leptons present in the standard model: the electron, the muon, and the tau. The neutrino is the lightest of the elementary fermions by a wide margin, and though observations indicate neutrinos are massive, currently only upper limits on the mass of individual neutrino types are known.

The first evidence for the existence of the neutrino came through the observation of the energy distribution of electrons emitted by nuclei undergoing  $\beta$ -decay. In 1930, Wolfgang Pauli postulated the existence of a light, electrically neutral particle as a solution to the problem of missing energy and momentum []. Confirmation of the existence of this proposed particle would not occur until 1956 through the detection of anti-electron neutrinos streaming from the nuclear fission reactors of the Savannah River Plant [11]. The maturation of particle detection techniques and instrumentation enabled the construction of vastly more sensitive experiments ultimately leading to the detection of neutrinos produced in cosmic ray air showers [] as well as from the interior of the Sun [].

### ***2.1 Interactions in Matter***

One of the defining characteristics of the neutrino is the ability to stream through large distances of ordinary matter unperturbed. However, neutrinos do occasionally interact with normal matter through several different interactions of varying complexity. The energy of the neutrino and the composition of the target material determine the most likely mode

of interaction. With that in mind, this section will only attempt to detail the neutrino-matter interaction of greatest importance in IceCube, i.e. the scattering of a neutrino with a target nucleon. While many other interaction processes can also occur (neutrino-electron scattering, inverse beta decay, coherent scattering with nuclei, etc.), the cross-section for these processes is far smaller than neutrino-nucleon scattering for neutrinos with energies of interest to IceCube and Deepcore ( $E_\nu \geq 10$  GeV).

### 2.1.1 Neutrino-Nucleon Scattering

### 2.1.2 Deep Inelastic Scattering

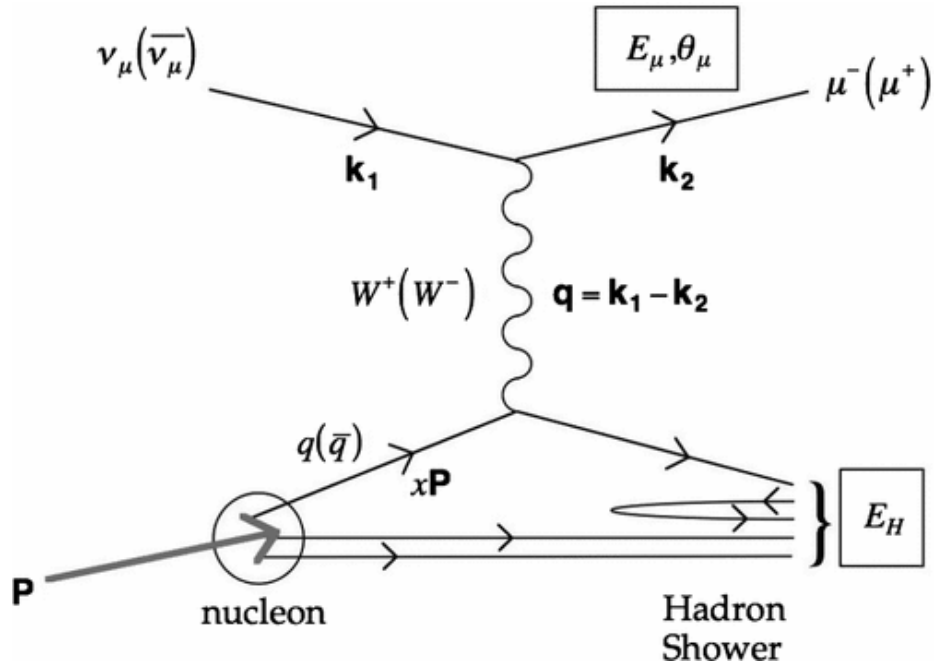
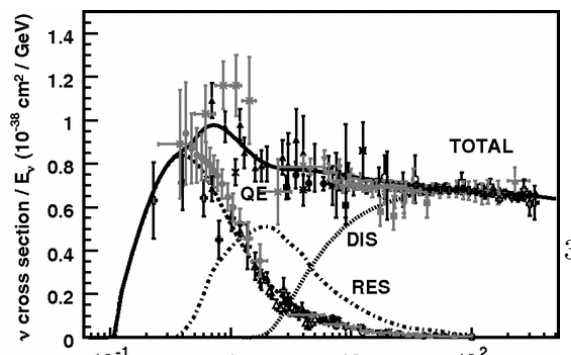


**Figure 2:** Feynman diagram of a  $\nu_\mu$  undergoing deep inelastic scattering with a nucleon via charged-current interaction. A large momentum exchange through a charged  $W$  boson leads to breakup of the nucleon.

### 2.1.3 Propagation of Interaction Products

The products leftover from high-energy neutrino-nucleon interactions are generally very energetic as well. These particles will



subsequently undergo many forms of energy loss and possible decay as they travel through a potential detection medium. In a given interaction, the total light yield and its spatial extent are contingent on the products of the interaction. The products themselves are ultimately determined by both the flavor of the primary neutrino and whether the neutrino interaction was of the charged- or neutral-current variety. This section will focus on how these secondaries interact and produce light and how that light propagates through glacial ice, the detection medium of IceCube.

For neutrinos of sufficient energy to be seen by IceCube, scattering with nucleons in the ice via either neutral or charged boson exchange will result in the breakup of the nucleon target.

## ***2.2 Flavor Oscillations***

## CHAPTER III

### NEUTRINO ASTRONOMY

The nascent field of neutrino astronomy

#### *3.1 Motivation*

The expansion of traditional optical astronomy into wavelengths unobservable to the human eye revealed myriad phenomena previously unknown to science. Use of wavebands of light spanning several orders of magnitude allowed for the discovery of completely new astronomical sources. Additionally, it allowed for the study of inherently different physical processes within and around source objects. Yet, for all the vast advances in our understanding of the universe the opening up of the electromagnetic spectrum has brought us, it relies entirely upon the physical properties of its messenger particle, the photon.

Absorption of light, either by intervening matter or other background photons, limits the number and type of source objects optical astronomy can hope to either observe or characterize. In order to explore regions of high density as well as very high-energy processes, entirely different methods of observation are required. The limitations imposed by light-based astronomy have led to the dedicated investigation of other particles and phenomena as potential cosmic messengers. This rapidly developing field, often referred to as multi-messenger astronomy, attempts to explore physical regions inaccessible to standard astronomy through the use of the highest energy cosmic rays, gravitational radiation, and high-energy neutrinos. These channels provide a unique window into the universe albeit each with their own detection challenges.

The neutrino in particular provides many excellent properties for potential use as an astrophysical messenger. Due to its very low probability of interaction, it is able to provide information from some of the densest regions within the interiors of sources. Additionally, neutrinos are able to stream freely as they propagate from their origin without suffering

absorption in intervening matter.

### ***3.2 Detection Methods***

The primary method for the detection of astrophysical neutrinos is through observation of Cerenkov light produced by interaction secondaries.

## CHAPTER IV

### NEUTRINO SOURCES

#### 4.1 Active Galactic Nuclei

#### 4.2 Gamma-ray Bursts

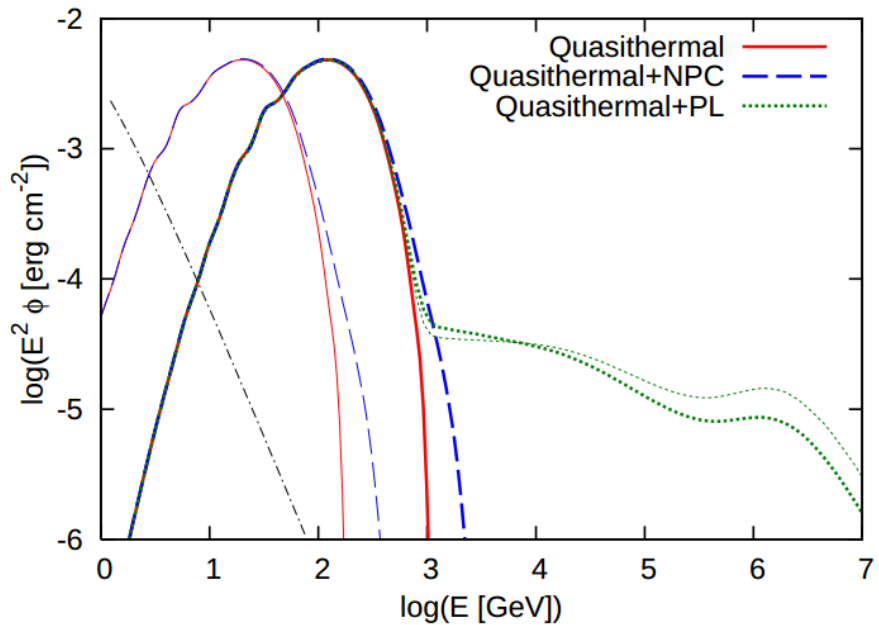


**Figure 3:** Energy Fluence of  $\nu_\mu$  and  $\bar{\nu}_\nu$  from high-luminosity GRB at a redshift of  $z=0.1$  [17]

#### 4.3 Core-Collapse Supernovae

The detection of several neutrino events in temporal coincidence with supernova 1987A marked the first detection of an extra-solar neutrino source. Neutrino events were observed in three separate detectors a few hours prior to the optical observation.

due to the close proximity of the progenitor in the Large Magellanic Cloud (approximately 50 kpc from Earth).

#### 4.4 Choked Gamma-ray Bursts

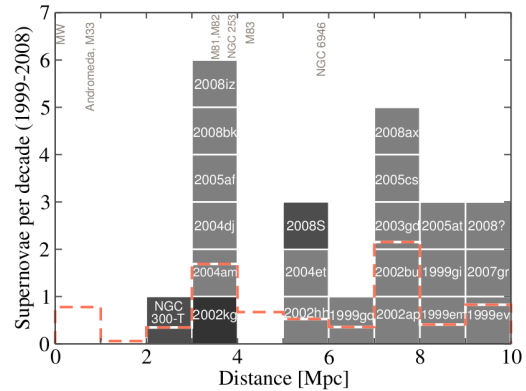


**Figure 4:** Observed SNe within 10 Mpc in the years 1999-2008 [16]

## CHAPTER V

### DETECTOR

#### *5.1 IceCube and IceTop*

The IceCube Neutrino Observatory [14] is km<sup>3</sup>-scale neutrino detector located deep within the glacial ice of the Antarctic ice sheet at the geographical South Pole. This location provides IceCube with a pristine detection medium in addition to mechanical support for the entirety of the array. The detector consists of 5,160 light sensors known as digital optical modules (DOMs) which are distributed along 86 cables (referred to as strings) that supply power and provide communication to the surface. Each cable is instrumented with 60 DOMs spaced 17 meters apart starting at 1450 meters below the surface and terminating at 2450 meters below. An inter-string spacing of 125 meters on average results in a total instrumented volume of approximately 1 km<sup>3</sup>. Figure 5 provides a schematic illustrating the detector geometry.

Installation of the IceCube strings took place over several years and required the use of a specialized hot-water drill. In the deployment process, the hot-water drill is used to bore through the ice leaving a water-filled column in which the string and its attached DOMs are lowered. The water column subsequently freezes the cable and all DOMs in place rendering them completely inaccessible from the surface. The deployment of the first IceCube string occurred on January 29th, 2005. The remaining strings were deployed over the next five summer seasons resulting in data seasons of different detector shapes and size. The final string was deployed on December 18, 2010 giving IceCube its ultimate 86-string configuration.

In addition to the detectors installed deep in the ice, there are also 81 surface detector stations (each station consisting of two tanks) at the surface. These tanks, which utilize two of the same light-sensing DOMs as IceCube, comprise the IceTop surface array. The DOMs in these tanks, which are also frozen in place, look for Cerenkov radiation produced

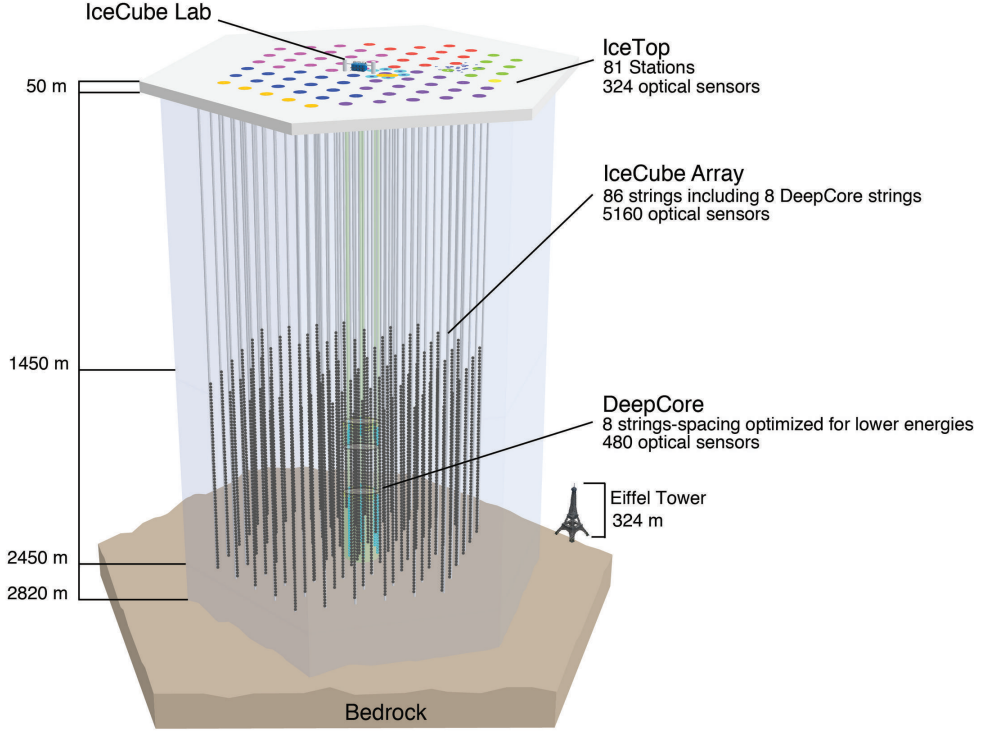


**Figure 5:** Diagram of the IceCube Neutrino Observatory (Courtesy of the IceCube Collaboration).

by cosmic ray air shower secondaries in the tank ice. By examining the arrival time of charged particles from the shower front, the direction of cosmic rays incident at Earth can be determined. The spatial extent of the shower as well as the total charge deposition in tank PMTs allows for accurate estimation of the energy of the primary cosmic ray. Data produced from IceTop is used to study cosmic ray composition, spectra, and anisotropy.

Due to the spatial relation of both IceTop and IceCube, they are able to complement the capabilities of each other quite nicely. IceTop's primary purpose is to study air shower physics, but it also serves as a veto for downgoing atmospheric muons and neutrinos in IceCube. This is particularly useful in the search for highly energetic neutrinos of astrophysical origin such as the events reported in [13] and [4]. Any downgoing events found by these searches that is accompanied by a causally connected air shower signal in IceTop is immediately identified as atmospheric in origin. Alternatively, the background muons

detected in IceCube can be used for more detailed study of air shower composition and energy in IceTop analyses. For more detailed information on the physics goals and detection capabilities of IceTop, see [7].

## 5.2 DeepCore

DeepCore [5] is a sub-detector deployed in tandem with IceCube between 2009 and 2010 primarily designed to lower the energy threshold of IceCube. The array consists of eight infill strings located in the center of the IceCube detector in addition to the first layer of surrounding standard IceCube strings. This configuration gives DeepCore three layers of IceCube strings to use as an active veto for the primary background of atmospheric muons. In order to improve detector response to lower energy neutrinos,  $\mathcal{O}(10\text{-}100 \text{ GeV})$ , the infill strings of DeepCore have a much closer inter-string separation ( 42 m) and have 50 DOMs spaced 7 m apart deployed deep in the ice between 2100 m and 2450 m. This denser instrumentation allows for better timing and spatial resolution of charged secondaries produced in neutrino interactions. Additional sensitivity to lower energies is gained through the use of the newer Hamamatsu R7081MOD model PMT in the infill string DOMs as opposed to the standard Hamamatsu R7081-02 used in IceCube. This model boasts higher quantum-efficiency in the photocathode for photons at typical Cerenkov wavelengths ( $\lambda \sim 400 \text{ nm}$ ). In-ice measurements of the high quantum efficiency (HQE) DOMs showed a 35% increase in sensitivity to Cerenkov light with respect to the standard IceCube DOMs [5].

The depth selected for deployment of the DeepCore DOMs was determined via examination of the ice properties previously mapped by both the Antarctic Muon and Neutrino Detector Array (AMANDA) [9] and pre-existing IceCube configurations [1]. These investigations into the optical properties of the ice revealed that the deepest ice ( $\leq 2100 \text{ m}$ ) had superior optical qualities with respect to the ice closer to the surface. Additionally, it was determined that a layer of high dust concentration in which light is scattered and absorbed to a much higher degree exists at a depth of 2000-2100 m. The eight infill strings also have a section of 10 DOMs with 10 m spacing located just above the dust layer. These DOMs form a veto cap to further increase the detection probability and rejection of directly

down-going muons. Figure 6 shows the distribution of DeepCore DOMs and the spacing and orientation of the DeepCore strings with respect to IceCube as a whole.

The primary physics goal of the DeepCore installation is to provide increased sensitivity for indirect dark matter searches by improving the IceCube detectors ability to resolve sub-100 GeV neutrino events. In this regard, it has been quite successful in establishing limits on the cross-sections of many WIMP (Weakly Interacting Massive Particle) dark matter models with the Sun [3] and Milky Way [6] as possible sources. The lowering of the detector’s energy threshold has also made neutrino oscillation parameter measurements possible due to the high statistics provided by atmospheric neutrino events [2]. Most importantly for the analysis presented in this thesis, however, is the improvement in effective area and resolution DeepCore provides for 30-150 GeV muon neutrinos. As this thesis will demonstrate, including these neutrino events into previously established IceCube point source analysis methods greatly improves IceCube’s capability to discover transient events with soft spectra.

### 5.3 *Neutrino Events in IceCube*

In order to isolate the sparse neutrino events from the abundance of background cosmic ray muons, it is necessary to fully understand the nature of the detector response to neutrinos and neutrino secondaries interacting within the detector. Neutrinos that are sufficiently energetic to be detected by IceCube will undergo deep inelastic scattering with a nucleon target (see for more information on this process see section 2.3.1). This process will either be charged-current (CC) or neutral-current (NC) depending on the nature of the boson exchange and the final lepton state. The hit topology of a given neutrino event in IceCube will depend upon the flavor of the neutrino ( $\nu_e$ ,  $\nu_\mu$ ,  $\nu_\tau$ ) as well as the channel through which it interacts with a target nucleon in the ice.

In NC interactions of all flavors, a hadronic cascade is produced which yields a roughly isotropic distribution of light. Any spatial extent in the hadronic cascade particles will be much smaller than the DOM separation distance. Thus, the Cerenkov emission from these particles will appear to be a point source of light within the detector. This results in a

spherical pattern of DOMs that register light from this type of interaction. The radius of DOMs which are able to detect light from the cascade is determined by the total energy deposited in the ice by the neutrino primary. Events with this hit pattern are referred to as cascades. An example event display for this type of interaction can be seen in figure 7.

Whereas the resultant hit pattern for NC interactions is flavor independent, the event topology in CC interactions is determined primarily by the lepton flavor of the neutrino. In addition to a hadronic cascade, the CC interaction will also yield an energetic lepton corresponding to the flavor of the interacting neutrino. In the case of  $\nu_e$  and  $\nu_\tau$  CC interactions, the resulting hit pattern in IceCube will take the form of a cascade in a similar manner to the NC interactions. While the source of Cerenkov emission is no longer point-like, the length of electron and tau particle tracks is much shorter than the inter-DOM separation distance. Some marginal pointing can be achieved for these events, however, since the light produced in the hadronic and electromagnetic cascades in these events is not totally symmetric. For sufficiently energetic  $\nu_\tau$  events in IceCube, more exotic signatures are possible. These arise from the increased lifetime of the outgoing  $\tau$  lepton resulting in two separate light-producing cascades that can be resolved separately either in space or time. As of the writing of this thesis, no events of this type have been observed in IceCube.

IceCube is designed specifically to be sensitive  $\nu_\mu$  CC interactions due to superior pointing provided by long-lived muon tracks in the ice. Daughter muons from  $\nu_\mu$  CC interactions can travel distances ranging from 300 m ( $E_{\nu_\mu} \sim 100$  GeV) to several kilometers ( $E_{\nu_\mu} \geq 1$  TeV) [15]. As these muons travel through the ice, they produce light in electromagnetic showers through both ionization and stochastic radiation losses. Because the muon is traveling faster than the speed of light in the ice ( $n_{ice} \sim 1.3$ ), the Cerenkov light generated about the muon track will form a cone which is ultimately aligned with the original neutrino direction. This results in a linear hit pattern in IceCube DOMs, providing a clear signal with good directional information. Muon tracks with the highest contained length in the detector provide the best resolution due to their long lever arm and low kinematic angular difference with respect to the parent neutrino. An example of a track event from a high-energy contained event search is shown in figure 8.

## Overhead View

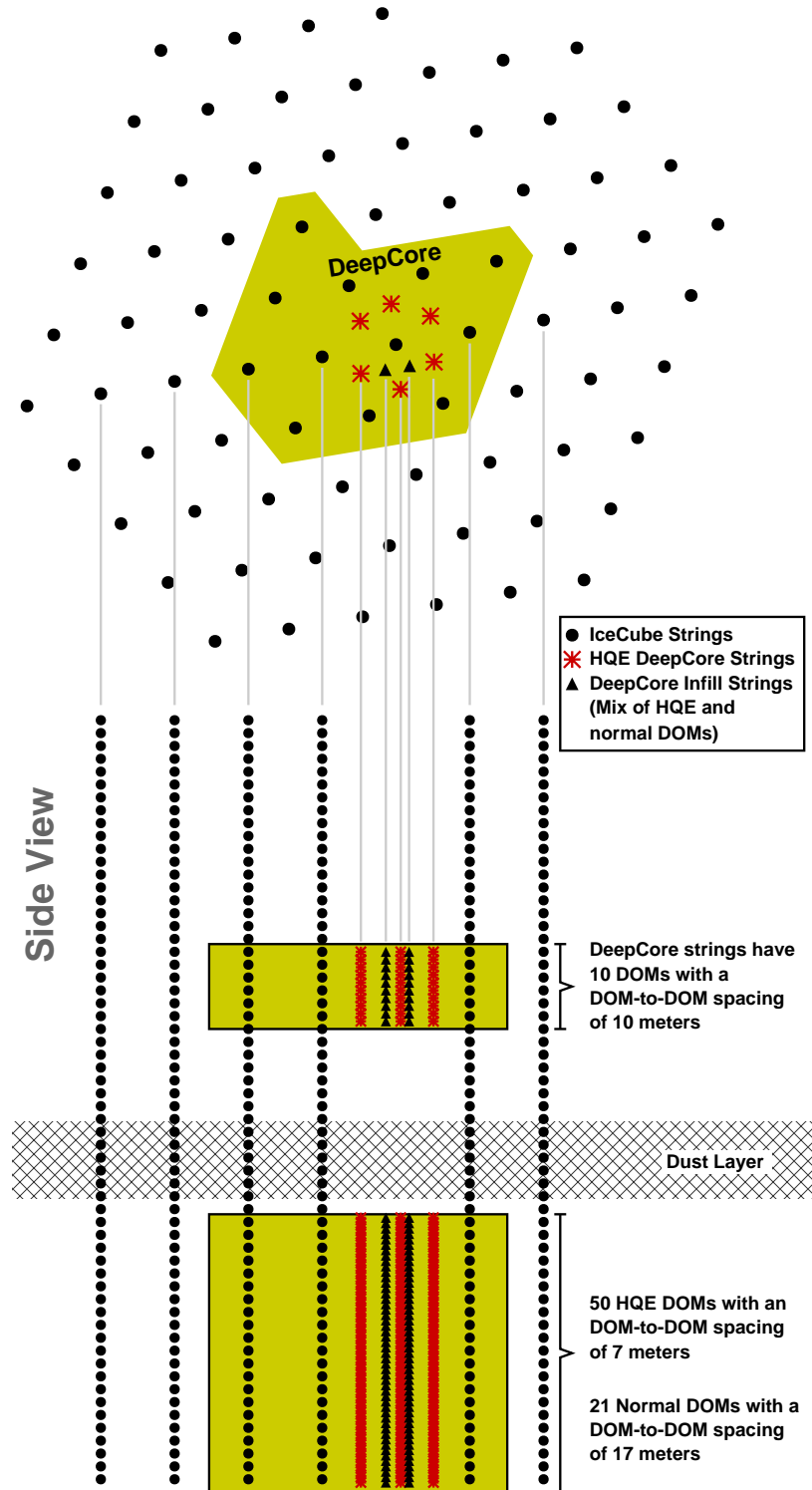


**Figure 6:** Top down and side-view diagram of DeepCore. The side-view shows the difference in DOM distribution for the infill strings and their relation to the dust layer [5].

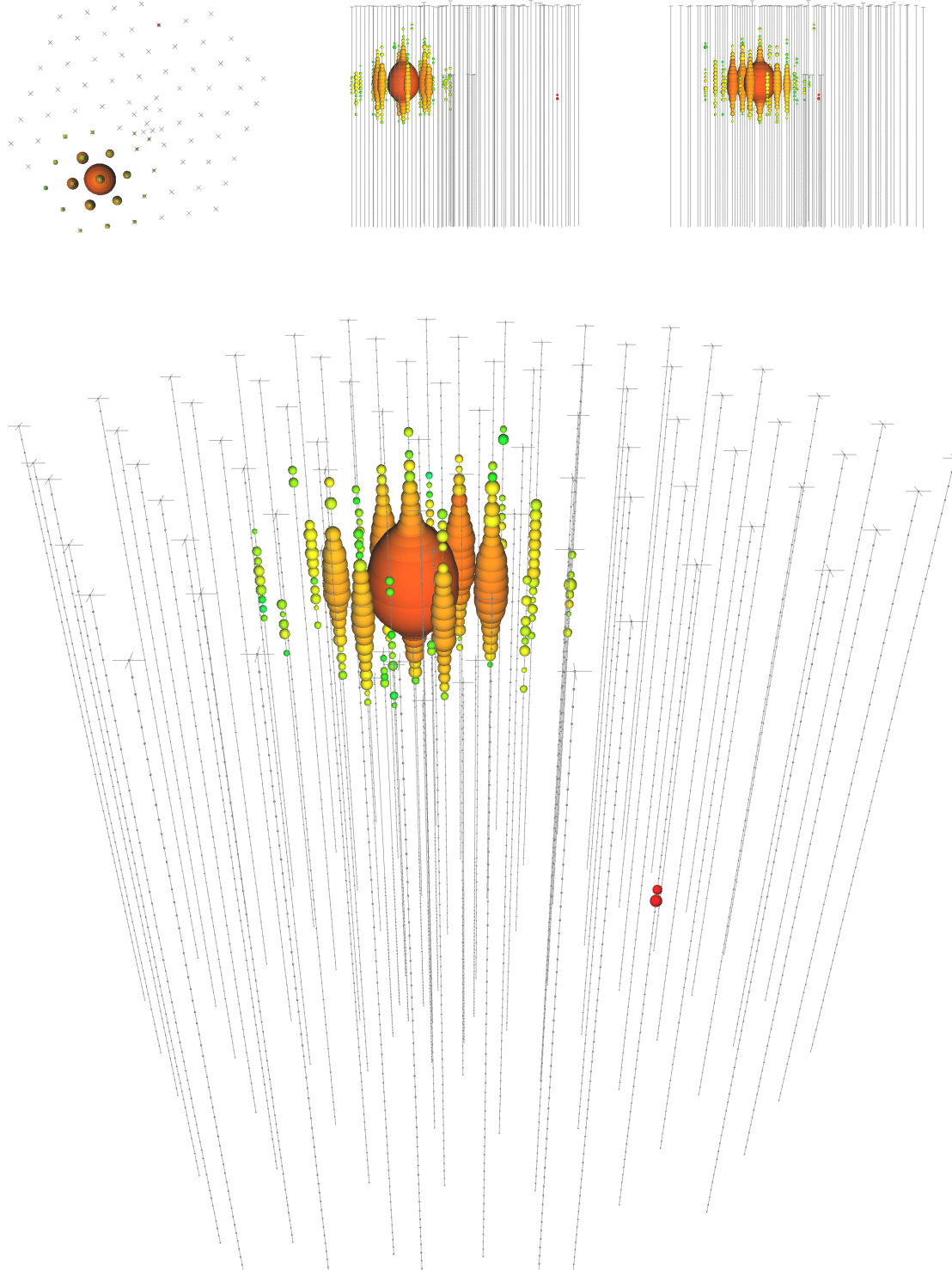


**Figure 7:** A high-energy cascade event in IceCube with deposited energy of  $210 \pm 29.0$  TeV [13]. The colored spheres represent DOMs that have registered light during the event. The size of the spheres are indicative of the total light received by the PMT on that DOM. The color denotes the timing of the hit with red corresponding to earlier times and blue corresponding to later times.

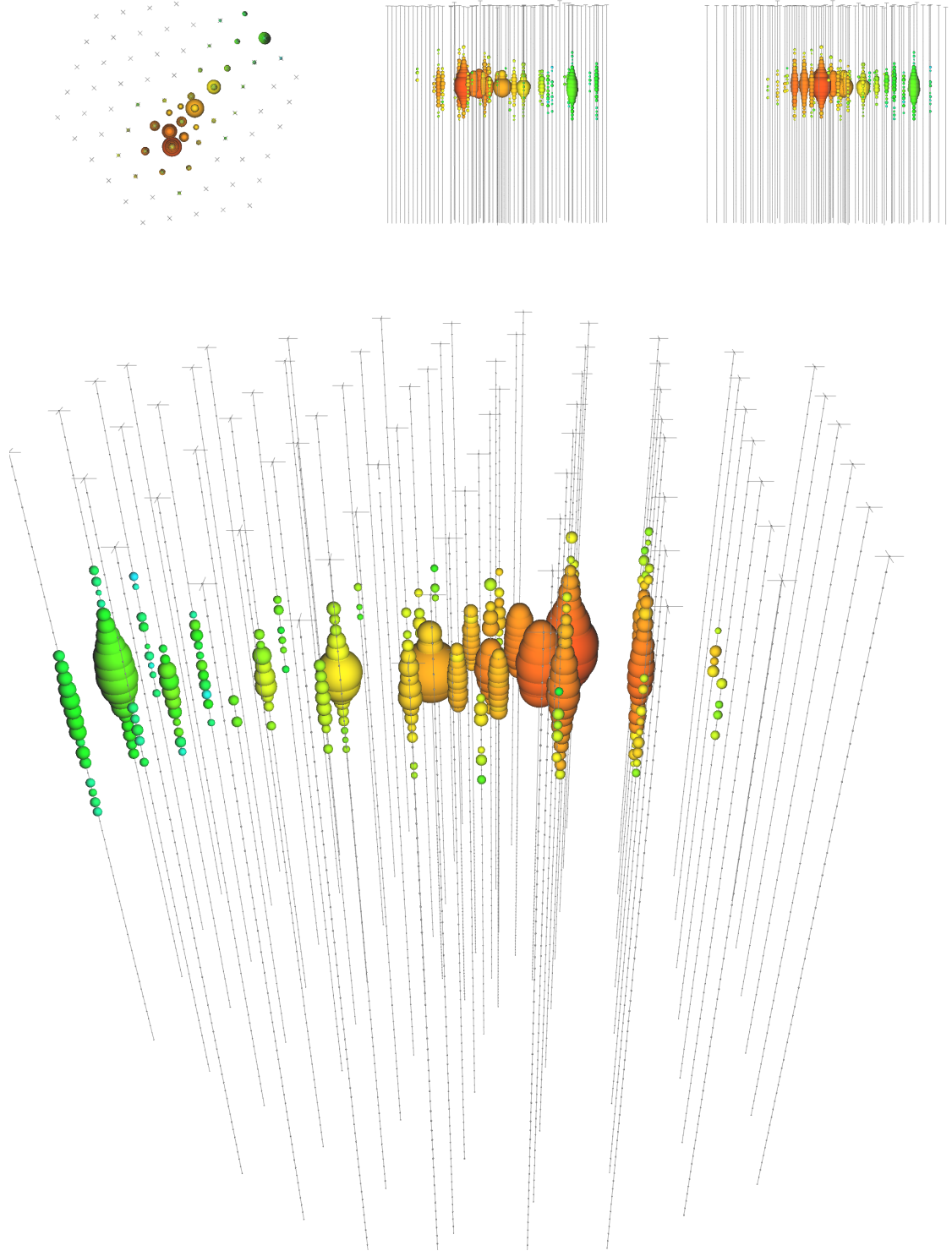


**Figure 8:** A high-energy track event in IceCube with deposited energy of  $71.4 \pm 9.0$  TeV [13]. The colored spheres represent DOMs that have registered light during the event. The size of the spheres are indicative of the total light received by the PMT on that DOM. The color denotes the timing of the hit with red corresponding to earlier times and blue corresponding to later times.

# CHAPTER VI

## DATA ACQUISITION

In this section, a succinct description of the detection of the light-yield from particle interactions in the ice and the subsequent processing of that data is given. The reader interested in a much more thorough account is encouraged to consult the summary by Abbasi et al. [8].

### 6.1 *The Digital Optical Module*

The essential component of the IceCube detector is the DOM. Each of these sensor units contains a Hamamatsu R7081-02 25 cm photo-multiplier tube (PMT), attached digitizing electronics, and LED flashers all housed within a glass pressure vessel [12]. A penetrator cable breaches the pressure vessel to connect the DOM electronics to the supporting string cable enabling DOM-to-DOM as well as DOM-to-surface communications.

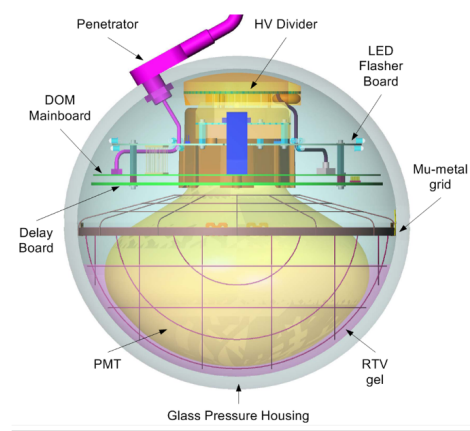


**Figure 9:** Schematic detailing DOM structure [8].

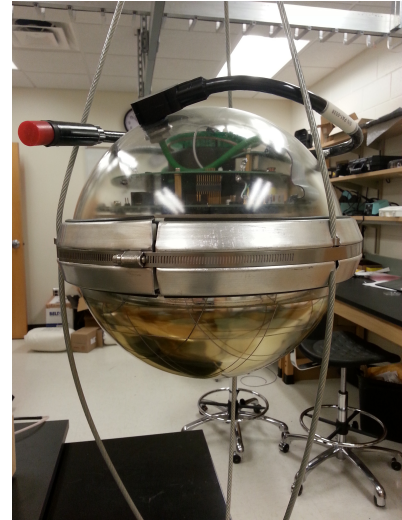


**Figure 10:** A fully assembled DOM supported by a cable harness.

Absolute quantum-efficiency measurements were made for all DOMs prior to deployment in the ice. In order to estimate how the efficiency might change after freeze-in, studies on

the efficiency of DOMs at typical in-ice temperatures were performed in labs at IceCube member institutions.

## ***6.2 Hit Generation***

All data acquisition begins with the registering and processing of photon hits in individual DOMs. Cerenkov photons from nearby passing charged secondaries are detected when they intercept the photocathode of the PMT on the underside of the DOM. This generates a small current pulse which is subsequently amplified

## ***6.3 Data Synchronization***

## ***6.4 Triggering and Event Building***

## CHAPTER VII

### EVENT SELECTION

A quick comparison between the rate at which atmospheric neutrinos trigger the IceCube and DeepCore detectors ( $\sim 10$  mHz) and the overall event rate ( $\sim 3$  kHz) readily shows that the data generated by IceCube is very strongly dominated by background. This background is almost entirely due to energetic muons produced in cosmic ray air showers passing through the detector from above. Due to the large range of physics capabilities of the detector, many different filters exist to reduce the data volume and select out events of interest to specific analyses.

#### *7.1 Low-energy Channel*

Because of the primary focus of this analysis on a lower-energy event selection, the DeepCore-dominated low-energy filter stream is taken as input. Selecting only events which pass this filter reduces the trigger-level data rate of 3 kHz to a much more manageable 37 Hz. The low-energy filter attempts to select a relatively background free sample by selecting a detection volume about DeepCore that does not extend to edge of the detector. This allows optical sensors outside of the detection volume to serve as dedicated downgoing muon detectors. Events that have hits on DOMs outside the defined detection volume that are causally correlated with the hits inside the volume are able to be identified as background muons. A schematic representation of this filtering algorithm is shown in ??.

This filter actually consists of two separate streams which are differentiated by the definition of which DOMs comprise the detection (or fiducial) volume and which DOMs are treated as belonging to the veto region.

## 7.2 Analysis Specific Cuts

### 7.2.1 Veto Cuts

### 7.2.2 Quality Cuts

### 7.2.3 Boosted Decision Tree

## 7.3 Event Reconstruction

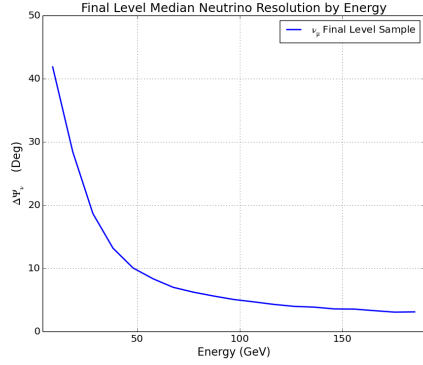


**Figure 11:** Median event resolution as a function of energy for simulation events passing all cuts.

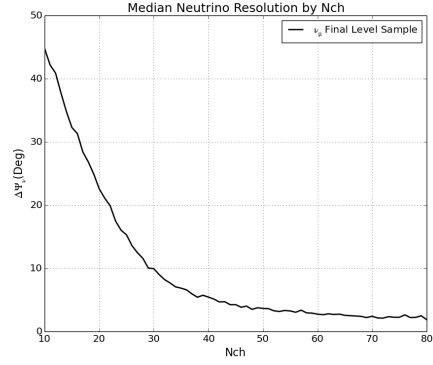


**Figure 12:** Median event resolution as a function of number of hit DOMs for simulation events passing all cuts.

## 7.4 Final Level Data

**Table 1:** Summary of final level event rates in mHz. The atmospheric muon and neutrino rates are estimated through the use of Monte Carlo simulation (MC).

Event Type	Rate (mHz)
Cosmic ray $\mu$	0.065
Atmospheric $\nu_\mu$	0.94
Total MC	1.001
Actual Data	0.774

LES Event 1

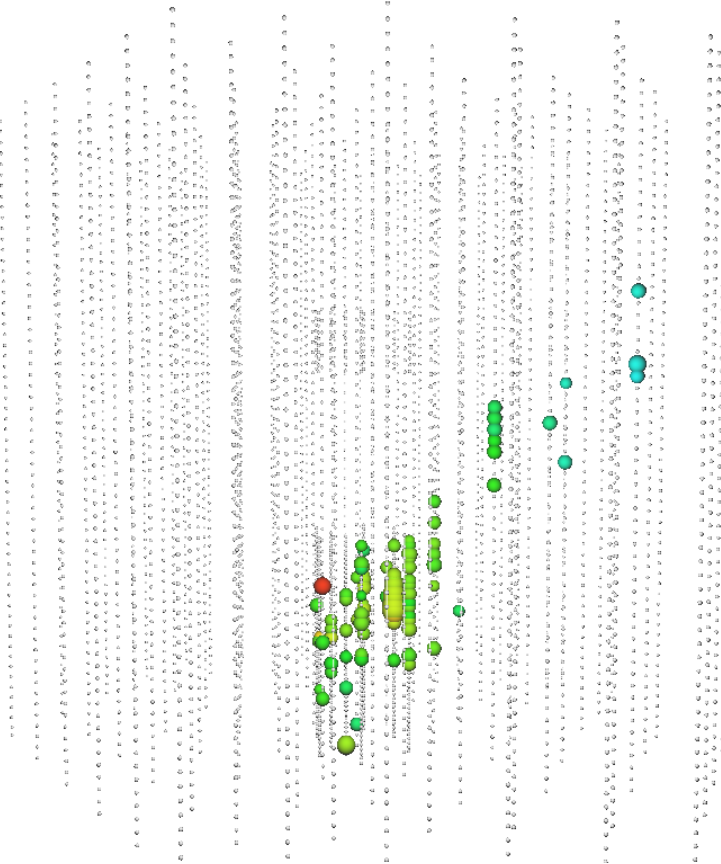


**Figure 13:** Event display for a final level neutrino track event originating in DeepCore. The colored spheres represent DOMs that have registered a hit during the event. The size of the spheres are indicative of the total light received by the PMT on that DOM. The color denotes the timing of the hit with red corresponding to earlier times and blue corresponding to later times.

# CHAPTER VIII

## ANALYSIS METHOD

The analysis presented in this thesis makes use of both directional and timing information from the final level event dataset. The techniques that are used in this analysis have been applied to other IceCube event selections in a similar fashion. As of yet, these time-dependent searches focused on IceCube events have yet to find any time-dependent neutrino sources of significance higher than background expectations []. A very thorough overview of the time-dependent likelihood analysis methods used in IceCube is given by Braun, et al. [10].

### 8.1 *Unbinned Likelihood Method*

$$S_i(|\mathbf{x}_i - \mathbf{x}_s|, t_i, t_o, \sigma_w) = \frac{\kappa}{4\pi \sinh \kappa} \exp(\kappa \cos |\mathbf{x}_i - \mathbf{x}_s|) * \frac{1}{\sqrt{2\pi}\sigma_w} \exp\left(-\frac{(t_i - t_o)^2}{2\sigma_w^2}\right) \quad (1)$$

$$B_i(\mathbf{x}_i, t_i) = P_{BkgDec}(\mathbf{x}_i) \frac{P_{BkgAz}(\delta_i, \alpha_i)}{T} \quad (2)$$

$$\mathcal{L}(\mathbf{x}_s, n_s, t_o, \sigma_w) = \prod P_i(|\mathbf{x}_i - \mathbf{x}_s|, n_s, t_i, t_o, \sigma_w) \quad (3)$$

$$\log \lambda = \log \left( \frac{\sqrt{2\pi}\hat{\sigma}_w}{T} \frac{\mathcal{L}(\mathbf{x}_s, \hat{n}_s, \hat{t}_o, \hat{\sigma}_w)}{\mathcal{L}(n_s = 0)} \right) \quad (4)$$

### 8.2 *Sky Scan*

The analysis performed is not a triggered search, and therefore it is necessary to examine the entire solid angle domain of the analysis for any possible transient sources. The difficulty in rejecting background muons at lower energies limits the analysis to up-going and horizontal events ( $< 5^\circ$  above the horizon). Because of IceCube's location at the South Pole, this results in a search over all right ascension in a declination band ranging from  $-5^\circ$  to  $90^\circ$ . The

search method discretizes the northern portion of the sky into many bins. The coordinates of these bins serve as the location of a hypothetical flaring source to be tested. The fairly large median resolution of the event sample (see Fig. 11) allows the size of the search bins to be set to a relatively coarse  $2^\circ$  by  $2^\circ$  in angular area.

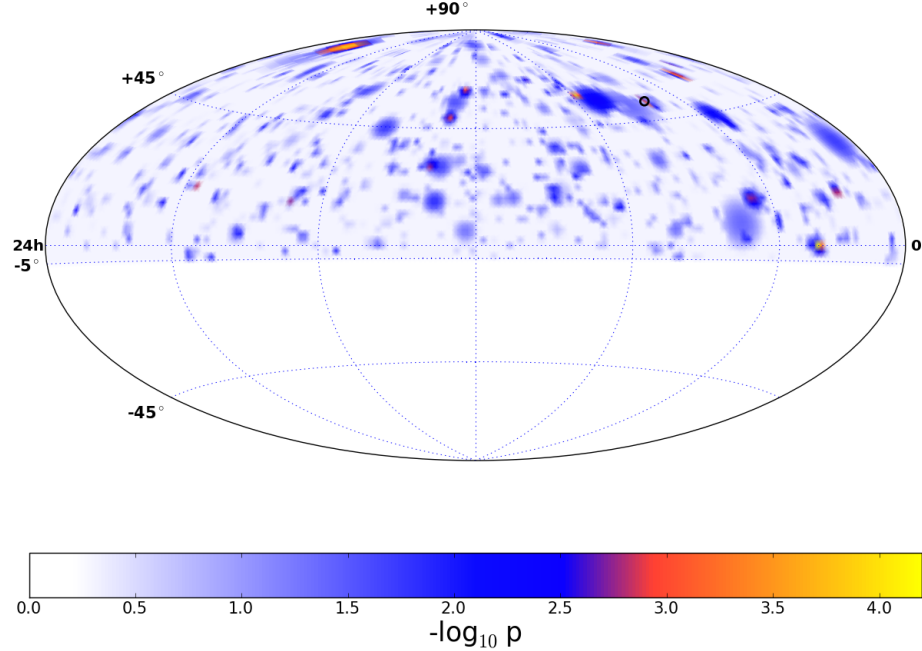


**Figure 14:** Randomized sky map of pre-trials p-values for best flares per bin. Random map generated by scrambling arrival times of real events. The black circle shows the location of the most significant flare found by the method.

### 8.3 Significance and Trials Factors

In order to determine which bin has the most significant flare, we evaluate an estimated p-value based on the maximized test statistic  $\lambda$  for that bin. The distribution of test statistic values for individual bins is not known *a priori* however.

# CHAPTER IX

## SYSTEMATIC EFFECTS

There are many systematic uncertainties that can affect the interpretation of the results of this analysis. The primary contributors to uncertainty being the *in situ* scattering and absorption properties of the ice medium and the absolute quantum efficiency of the PMTs within the DOMs.

### ***9.1 Ice Properties***

### ***9.2 DOM Quantum Efficiency***

# CHAPTER X

## RESULTS

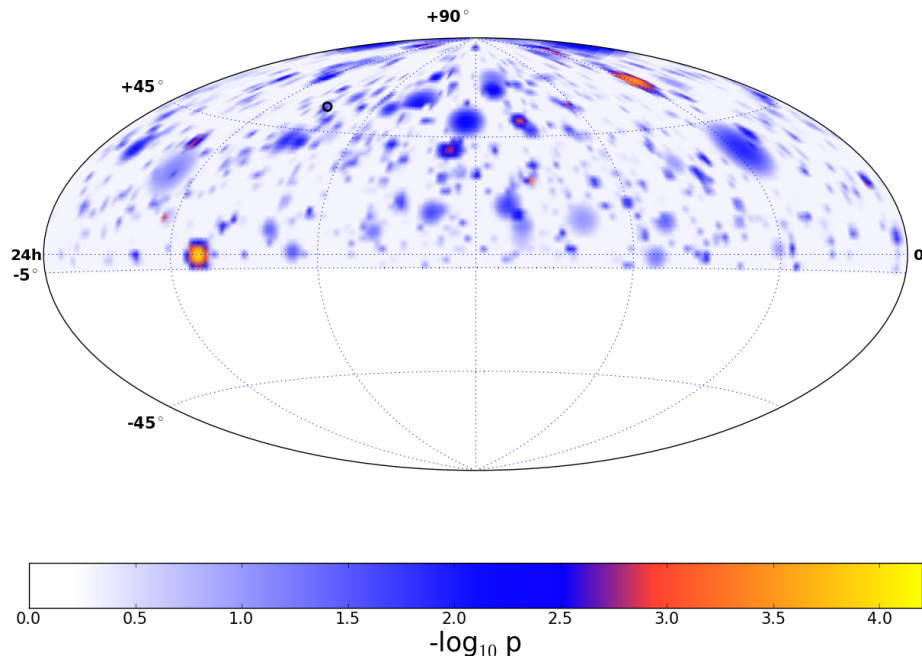


**Figure 15:** Sky map of pre-trials p-values for best flares per bin. The black circle identifies the location of the most significant flare found at RA = 268.75° and Declination = 54.25°.

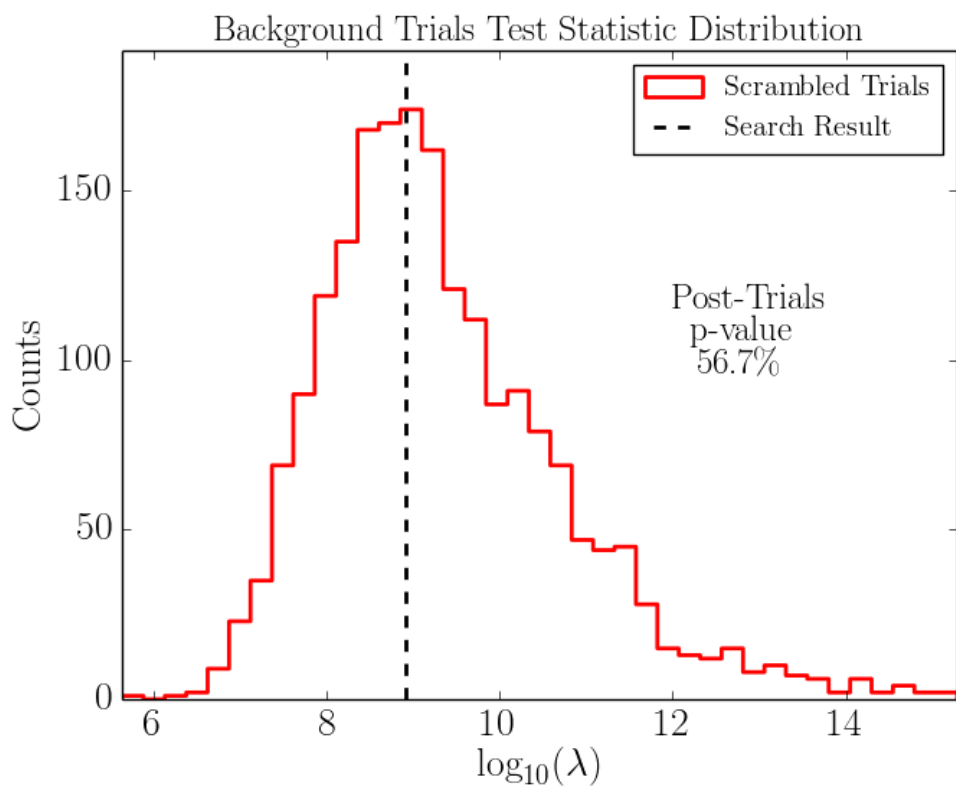


**Figure 16:** Distribution of test statistic  $\lambda$  of most significant flare found in 1,985 background trials. The test statistic value for the best fit flare on the unscrambled data set is also plotted.

## **CHAPTER XI**

### **INTERPRETATION**

## **CHAPTER XII**

### **CONCLUSION**

## **APPENDIX A**

### **APPENDIX A – FINAL LEVEL EVENT DISTRIBUTIONS**

## REFERENCES

- [1] “South Pole glacial climate reconstruction from multi-borehole laser particulate stratigraphy,” *Journal of Glaciology*, vol. 59, pp. 1117–1128, 2013.
- [2] AARTSEN, M. G., ABBASI, R., ABDOU, Y., ACKERMANN, M., ADAMS, J., AGUILAR, J. A., AHLERS, M., ALTMANN, D., AUFFENBERG, J., BAI, X., and ET AL., “Measurement of Atmospheric Neutrino Oscillations with IceCube,” *Physical Review Letters*, vol. 111, p. 081801, Aug. 2013.
- [3] AARTSEN, M. G., ABBASI, R., ABDOU, Y., ACKERMANN, M., ADAMS, J., AGUILAR, J. A., AHLERS, M., ALTMANN, D., AUFFENBERG, J., BAI, X., and ET AL., “Search for Dark Matter Annihilations in the Sun with the 79-String IceCube Detector,” *Physical Review Letters*, vol. 110, p. 131302, Mar. 2013.
- [4] AARTSEN, M. G., ACKERMANN, M., ADAMS, J., AGUILAR, J. A., AHLERS, M., AHRENS, M., ALTMANN, D., ANDERSON, T., ARGUELLES, C., ARLEN, T. C., and ET AL., “Observation of High-Energy Astrophysical Neutrinos in Three Years of IceCube Data,” *Physical Review Letters*, vol. 113, p. 101101, Sept. 2014.
- [5] ABBASI, R., ABDOU, Y., ABU-ZAYYAD, T., ACKERMANN, M., ADAMS, J., AGUILAR, J. A., AHLERS, M., ALLEN, M. M., ALTMANN, D., ANDEEN, K., and ET AL., “The design and performance of IceCube DeepCore,” *Astroparticle Physics*, vol. 35, pp. 615–624, May 2012.
- [6] ABBASI, R., ABDOU, Y., ABU-ZAYYAD, T., ADAMS, J., AGUILAR, J. A., AHLERS, M., ANDEEN, K., AUFFENBERG, J., BAI, X., BAKER, M., and ET AL., “Search for dark matter from the Galactic halo with the IceCube Neutrino Telescope,” *Phys. Rev. D*, vol. 84, p. 022004, July 2011.

- [7] ABBASI, R., ABDOU, Y., ACKERMANN, M., ADAMS, J., AGUILAR, J. A., AHLERS, M., ALTMANN, D., ANDEEN, K., AUFFENBERG, J., BAI, X., and ET AL., “IceTop: The surface component of IceCube. The IceCube Collaboration,” *Nuclear Instruments and Methods in Physics Research A*, vol. 700, pp. 188–220, 2013.
- [8] ABBASI, R., ACKERMANN, M., ADAMS, J., AHLERS, M., AHRENS, J., ANDEEN, K., AUFFENBERG, J., BAI, X., BAKER, M., BARWICK, S. W., and ET AL., “The IceCube data acquisition system: Signal capture, digitization, and timestamping,” *Nuclear Instruments and Methods in Physics Research A*, vol. 601, pp. 294–316, 2009.
- [9] ACKERMANN, M., AHRENS, J., BAI, X., BARTELT, M., BARWICK, S. W., BAY, R. C., BECKA, T., BECKER, J. K., BECKER, K.-H., BERGHAUS, P., BERNARDINI, E., BERTRAND, D., BOERSMA, D. J., BÖSER, S., BOTNER, O., BOUCHTA, A., BOUHALI, O., BURGESS, C., BURGESS, T., CASTERMANS, T., CHIRKIN, D., COLLIN, B., CONRAD, J., COOLEY, J., COWEN, D. F., DAVOUR, A., DE CLERCQ, C., DE LOS HEROS, C. P., DESIATI, P., DE YOUNG, T., EKSTRÖM, P., FESER, T., GAISSER, T. K., GANUGAPATI, R., GEENEN, H., GERHARDT, L., GOLDSCHMIDT, A., GROSS, A., HALLGREN, A., HALZEN, F., HANSON, K., HARDTKE, D. H., HARENBERG, T., HAUSCHILD, T., HELBING, K., HELLWIG, M., HERQUET, P., HILL, G. C., HODGES, J., HUBERT, D., HUGHEY, B., HULTH, P. O., HULTQVIST, K., HUNDERTMARK, S., JACOBSEN, J., KAMPERT, K. H., KARLE, A., KESTEL, M., KOHNEN, G., KÖPKE, L., KOWALSKI, M., KUEHN, K., LANG, R., LEICH, H., LEUTHOLD, M., LIUBARSKY, I., LUNDBERG, J., MADSEN, J., MARCINIEWSKI, P., MATIS, H. S., MC PARLAND, C. P., MESSARIUS, T., MINAEVA, Y., MIOČINOVIĆ, P., MORSE, R., MÜNICH, K., NAHNHAUER, R., NAM, J. W., NEUNHÖFFER, T., NIESSEN, P., NYGREN, D. R., OLBRECHTS, P., POHL, A. C., PORRATA, R., PRICE, P. B., PRZYBYLSKI, G. T., RAWLINS, K., RESCONI, E., RHODE, W., RIBORDY, M., RICHTER, S., RODRÍGUEZ MARTINO, J., SANDER, H.-G., SCHLENSTEDT, S., SCHNEIDER, D., SCHWARZ, R., SILVESTRI, A., SOLARZ, M., SPICZAK, G. M., SPIERING, C., STAMATIKOS, M., STEELE, D., STEFFEN, P., STOKSTAD, R. G., SULANKE, K.-H., TABOADA, I.,

TARASOVA, O., THOLLANDER, L., TILAV, S., WAGNER, W., WALCK, C., WALTER, M., WANG, Y.-R., WIEBUSCH, C. H., WISCHNEWSKI, R., WISSING, H., and WOSCHNAGG, K., “Optical properties of deep glacial ice at the South Pole,” *Journal of Geophysical Research (Atmospheres)*, vol. 111, p. 13203, July 2006.

- [10] BRAUN, J., BAKER, M., DUMM, J., FINLEY, C., KARLE, A., and MONTARULI, T., “Time-dependent point source search methods in high energy neutrino astronomy,” *Astroparticle Physics*, vol. 33, pp. 175–181, Apr. 2010.
- [11] COWAN, JR., C. L., REINES, F., HARRISON, F. B., KRUSE, H. W., and MCGUIRE, A. D., “Detection of the Free Neutrino: A Confirmation,” *Science*, vol. 124, pp. 103–104, July 1956.
- [12] HANSON, K. and TARASOVA, O., “Design and production of the IceCube digital optical module,” *Nuclear Instruments and Methods in Physics Research A*, vol. 567, pp. 214–217, Nov. 2006.
- [13] ICECUBE COLLABORATION, “Evidence for High-Energy Extraterrestrial Neutrinos at the IceCube Detector,” *Science*, vol. 342, Nov. 2013.
- [14] ICECUBE COLLABORATION, ACHTERBERG, A., ACKERMANN, M., ADAMS, J., AHRENS, J., ANDEEN, K., ATLEE, D. W., BACCUS, J., BAHCALL, J. N., BAI, X., and ET AL., “First year performance of the IceCube neutrino telescope,” *Astroparticle Physics*, vol. 26, pp. 155–173, Oct. 2006.
- [15] IYER DUTTA, S., RENO, M. H., SARCEVIC, I., and SECKEL, D., “Propagation of muons and taus at high energies,” *Physical Review D*, vol. 63, p. 094020, May 2001.
- [16] KISTLER, M. D., YÜKSEL, H., ANDO, S., BEACOM, J. F., and SUZUKI, Y., “Core-collapse astrophysics with a five-megaton neutrino detector,” *Phys. Rev. D*, vol. 83, p. 123008, June 2011.

- [17] MURASE, K., KASHIYAMA, K., and MÉSZÁROS, P., “Subphotospheric Neutrinos from Gamma-Ray Bursts: The Role of Neutrons,” *Physical Review Letters*, vol. 111, p. 131102, Sept. 2013.

## **INDEX**

## VITA